



# The Fast and the Capacious: A [Ni(Salen)]-TEMPO Redox-Conducting Polymer for Organic Batteries

Anatoliy A. Vereshchagin<sup>+[a]</sup>, Daniil A. Lukyanov<sup>+[a]</sup>, Ilia R. Kulikov,<sup>[b]</sup> Naitik A. Panjwani,<sup>[b]</sup> Elena A. Alekseeva,<sup>[a]</sup> Jan Behrends,<sup>[b]</sup> and Oleg V. Levin<sup>\*[a]</sup>

Redox-active nitroxyl-containing polymers are promising candidates as possible replacements for inorganic based energy-storage materials, due to their high energy density and fast redox kinetics. One challenge towards the implementation of such a system is the insufficient electrical conductivity, impeding the charge collection even with highly conductive additives. Herein, the first implementation of a polymeric bis(salicylideneiminato) nickel (NiSalen) conductive backbone as an active charge-collecting wire is reported. NiSalen simultane-

ously serves as a charge collector for nitroxyl pendants and supports the redox capacity of the material. This novel polymer exhibits a specific capacity of up to  $91.5 \text{ mAh g}^{-1}$ , retaining 87% of its theoretical capacity at 800 C and more than 30% at as high as 3000 C (66% capacity retention after 2000 cycles). The properties of the new material upon operation was studied by means of *operando* electrochemical methods, UV-Vis, and electron paramagnetic resonance spectroscopy.

## 1. Introduction

Batteries and supercapacitors based on redox polymers represent a promising class of future electrochemical power sources.<sup>[1]</sup> A growing interest is focused on nitroxyl-based polymers, which approach the theoretical capacities comparable to high-energy batteries and possess the fast redox kinetics and stability inherent to high-power supercapacitors.<sup>[2]</sup> Since the first report of rechargeable batteries with a nitroxyl-containing polymeric cathode,<sup>[3]</sup> a number of nitroxyl-containing materials have been developed, featuring high specific energy<sup>[4]</sup> and power,<sup>[5]</sup> as well as perfect cycling stability.<sup>[6]</sup>

In nitroxyl-based polymers the only charge-transport pathway is electron hopping between adjacent redox centers, which is fast on the microscopic scale. Despite this, the macroscopic electron conductivity of nitroxyl-based material appears to be very low. Therefore, additional components are usually introduced into the electrode composition to set the electronic conductivity of the nitroxyl-containing materials at a level that assures the complete utilization of its energy storage potential. High conductivity may be achieved by introduction of carbonaceous materials,<sup>[7]</sup> which act as a "dead mass" and decrease the overall energy density of the electrode. Another

possibility for increasing the conductivity of redox polymers is to improve the electrical conductivity of the main chain by using conductive polymers as a backbone.<sup>[8]</sup> The materials of such architecture are called conductive redox polymers (CRP). Several types of nitroxyl-containing CRPs based on different backbones such as polyaniline,<sup>[9]</sup> polyacetylene,<sup>[10]</sup> polypyrrole<sup>[11]</sup> and polythiophenes<sup>[12]</sup> are described in the literature. However, the energy and power densities of these materials do not come together (see Electronic Supplementary Information, Chapter „Micro-review on nitroxyl-containing CRPs“ for details). To combine the desired energy, power and stability in a single material, the fine tuning of key factors affecting the performance of CRPs, such as linker configuration<sup>[12d,13]</sup> and redox-matching between the backbone and pendant group,<sup>[14]</sup> should be carried out, which requires the development of novel conductive backbones and grafting approaches.

Polymeric bis(salicylideneiminato) complexes of transition metals (MSalens) represent a class of conductive polymers with distinct properties. Specifically, polymeric Salen complexes based on nickel have a large reversible electroactivity window, perfectly matching the TEMPO/TEMPO<sup>+</sup> redox potential (anodic limit of electroactivity reaches 4.3 V vs Li/Li<sup>+</sup>),<sup>[15]</sup> and a conductivity up to  $100 \text{ Scm}^{-1}$ ,<sup>[16]</sup> while their specific redox capacitance and energy density (ca.  $330 \text{ Jg}^{-1}$ )<sup>[17]</sup> exceed those of most conductive polymers. The electrochemical properties of these complexes may be easily tuned by variation of the substituents occupying the ligand bridge, imine functionalities and the aromatic core.<sup>[18]</sup> As a result, NiSalens are promising materials for energy storage devices such as hybrid supercapacitors.<sup>[19]</sup>

One may conclude that the polymer Salen complexes of nickel are not inferior to the classical conductive polymers regarding stability and electrical conductivity, but surpass them in capacitance. Based on the above knowledge, we suggest that using NiSalen type polymer complexes as a conductive

[a] A. A. Vereshchagin,<sup>+</sup> Dr. D. A. Lukyanov,<sup>+</sup> Dr. E. A. Alekseeva, Prof. O. V. Levin

Saint Petersburg University

7/9 Universitetskaya nab., St. Petersburg, 199034, Russian Federation

E-mail: o.levin@spbu.ru

[b] I. R. Kulikov, Dr. N. A. Panjwani, Prof. J. Behrends

Berlin Joint EPR Lab, Fachbereich Physik

Freie Universität Berlin

14195 Berlin, Germany

<sup>†</sup> These authors contributed equally to this work

Supporting information for this article is available on the WWW under <https://doi.org/10.1002/batt.202000220>

polymer framework for TEMPO-containing materials of lithium-ion batteries is a new and promising approach on the route towards the design of organic cathodes with high conductivity and specific capacity. Recently the evidence of the synergistic action of polymeric NiSalen with the nitroxyl polymer PTMA in a composite has been demonstrated, indicating the prospective of such a class of conducting polymers for energy purposes.<sup>[20]</sup>

Herein we report the first redox-conductive polymer with a NiSalen backbone and 2,2,6,6-tetramethylpiperidin-1-oxyl-4-yl (TEMPO) pendants. The succinyl linker was chosen to connect the TEMPO groups to the backbone because of preparative reasons. TEMPOL is the most accessible TEMPO-containing building block. Acylation of alcohols and phenols are highly reliable transformations which may be conducted in mild conditions. This is important for the proof of concept study involving labile fragments such as the NiSalen complex. The NiSalen monomers bearing nitroxyl pendants were obtained and subjected to anodic electrochemical oxidation, resulting in films of the redox-conductive polymeric materials directly on metal electrodes. The electrochemical and spectroelectrochemical behavior of the obtained material was studied using cyclic voltammetry (CV), electrochemical quartz crystal microbalance (EQCM), chronoamperometric charge/discharge (GCD), as well as, operando conductivity measurements, UV-Vis and Electron Paramagnetic Resonance (EPR) spectroscopy.

## 2. Results and Discussion

### 2.1. Synthesis and Characterizations of the Monomers

The di-TEMPO NiSalen complex, DiTS, was synthesized in two steps with 35% overall yield (Figure 1) by the acylation of 2,3-dihydroxybenzaldehyde with succinyl ester of TEMPOL followed by its condensation with ethylene diamine and complexation with nickel ion. The FTIR spectrum of DiTS shows two vibrational modes around 1735–1760 cm<sup>-1</sup>, characteristic for esters, and a signal at 1454 cm<sup>-1</sup> from nitroxyl fragments, supporting the presence and connectivity of TEMPOL-succinyl pendant, along with strong vibration at 1624 cm<sup>-1</sup> attributed to the endocyclic C=N bond and broad band at 739 cm<sup>-1</sup>, typical for Ni–O and Ni–N complexes. HRMS-ESI spectra confirm the elemental composition of product, containing only the [M + Na]<sup>+</sup> signal, which indicates the strong coordination of Na<sup>+</sup> ion into the O<sub>4</sub> cavity. NMR spectra of the monomer were

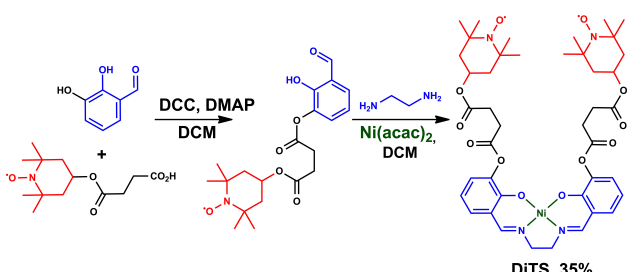


Figure 1. Scheme for the synthesis of DiTS.

recorded after in situ quenching of the paramagnetic centers with ascorbic acid. The DiTS complex shows characteristic signals at 1.08 ppm which correspond to CH<sub>3</sub> groups of TEMPO, a set of signals in the 1.44–3.74 ppm region from CH and CH<sub>2</sub>-groups of the TEMPO-succinyl moiety, a signal at 3.44 ppm from the ethylene bridge of the complex as well as three signals in the aromatic region.

### 2.2. Electrochemical Polymer Deposition

Electrochemical polymerization of DiTS was studied by means of the EQCM technique on piezoelectric crystals coated with platinum using a linear voltage sweep. The CV of DiTS (Figure 2A) shows the paired peaks A and A' at 0.55 V and 0.47 V respectively, which correspond to charging and discharging of the nitroxyl fragments. An irreversible anodic peak B corresponds to oxidative coupling of the NiSalen fragments of DiTS, which results in the polymer p-DiTS.<sup>[20–21]</sup> The gradual increase of the CV current and the electrode mass (Figure 2A) in the subsequent cycles indicates the course of the polymerization process. An unusual feature in the EQCM curves, recorded during the electropolymerization process, is that the mass growth at the electrode occurs predominantly at potentials below the peak A' (Figure 2A), which is in contradiction to previous reports on the deposition of a NiSalen-type polymer, where polymerization occurs at potentials above the oxidation peak of the monomeric NiSalen.<sup>[22]</sup>

The CV sweep boundaries were varied to establish the optimal conditions for the polymerization of DiTS. Only the redox peaks of the TEMPO moieties in solution are observed on CV (Figure 2C, curve i) while sweeping in –0.40–0.75 V range without polymer formation. An extension of the anodic boundary to 0.90 V (Figure 2C, curve ii) led to an increase in EQCM mass and CV current, which indicates the polymer growth on the electrode surface. Further extension of the anodic region of the CV range (Figure 2C, curve iv) did not improve the polymerization process, but led to a decrease of the conductivity of the film due to overoxidation (Figure S4), highlighting 0.90 V as an optimal position of the anodic boundary. While polymerization is possible at higher potentials on the surface of a clean substrate, low conductivity of the overoxidized film is blocking further monomer oxidation on the surface, leading to rapid decrease in monomer oxidation current (Figure S4 and Figure 2C, curve iv). When the cathodic boundary was set near the A/A' pair and the CV was performed between 0.35 V and 0.90 V (Figure 2C, curve iii), no polymerization occurred, emphasizing the crucial role of the charge/discharge of the nitroxyl fragments in the polymerization process.

The conventional mechanism for the chain growth of polymeric NiSalens is based on the formation of radical cation species. Although the NiSalen-centered radical cations of DiTS are formed on the peak B (Figure 2A), apparently the polymerization proceeds at a low rate in this area of potentials, compared to other NiSalen type complexes.<sup>[22]</sup> Based on the obtained results, we assume that the positive charge density

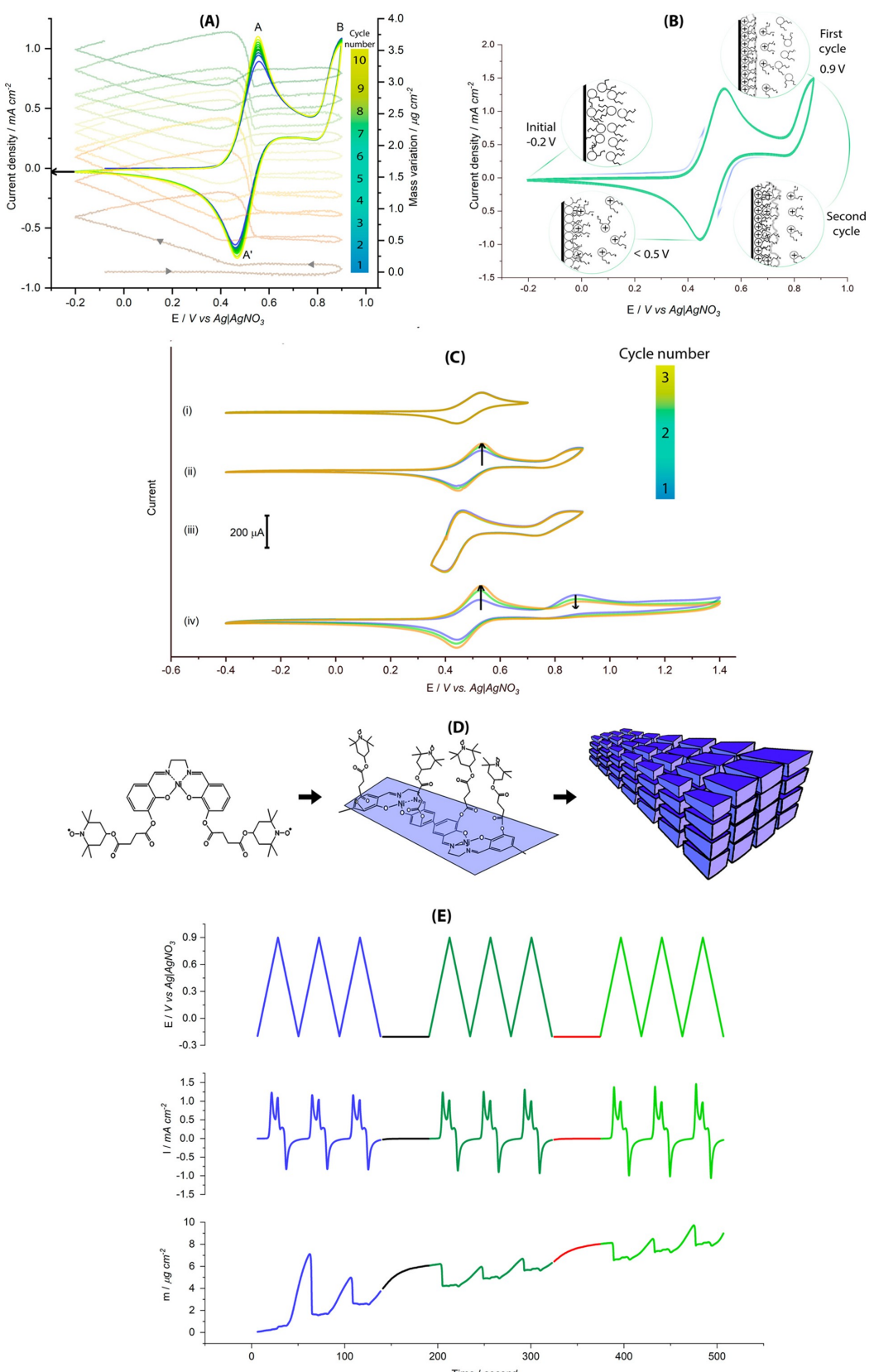


**Figure 2.** QCM analysis of the polymerization of DiTS (1 mM solution) in 0.1 M  $\text{Et}_4\text{NBF}_4$  in  $\text{CH}_3\text{CN}$  with a scan rate of 50 mVs<sup>-1</sup> (A); Scheme of the TEMPO "shield" forming during electropolymerization (B); CV of the synthesis of p-DiTS from 0.1 M  $\text{Et}_4\text{NBF}_4$  in  $\text{CH}_3\text{CN}$  at variable potential range with 50 mVs<sup>-1</sup> scan rate (C); Scheme of the polymer formation process (D); EQCM analysis of the synthesis of p-DiTS in 0.1 M  $\text{Et}_4\text{NBF}_4/\text{CH}_3\text{CN}$  for standard potential ranges with 50 mVs<sup>-1</sup> scan rate using CV/PStat reduction during 200 seconds mode (E).

both on the monomer molecules and deposited polymer layers grow rapidly above the A (Figure 2A) peak potential due to simultaneous oxidation of the NiSalen core and two TEMPO fragments in one molecule. High charge density causes intermolecular coulombic repulsion, acting as a coulombic "shield", which hinders the coupling of radical cation species and prevents the chain growth. As soon as the potential has decreased to the A' (Figure 2A) peak on the negative scan of the CV (Figure S5C, point C), rapid polymer growth occurred due to the discharge of the p-DiTS film, which deactivates the coulombic shield. The formation of the polymer proceeds until the shield recovers during the next CV cycle due to the oxidation of nitroxyl fragments. At this point, a sharp decrease in mass occurs due to the desorption of the monomeric DiTS molecules repelled by the charging coulombic shield. The scheme of this process is depicted in Figure 2B and a scheme of the polymer formation process in Figure 2D.

To verify the proposed mechanism, an additional experiment was conducted. A constant potential of  $-0.2\text{ V}$  was applied for 200 seconds using potentiostatic mode between every three cycles of the CV polymerization, and the change in mass was measured simultaneously (Figure 2E). As illustrated, this mode does not lead to significant changes in the polymerization rate, as compared to normal CV cycles. Most likely, the charged monomers that were collected near the electrode surface during oxidation simply have had additional 200 s for a more complete reaction with the polymer, yet no new active species were produced at  $-0.2\text{ V}$ . The proposed mechanism of polymerization is substantially different from the behavior of other NiSalen type molecules,<sup>[22]</sup> so additional experiments were carried out using CV mode with the optimal potential range but at sweep potential rate of  $5\text{ mVs}^{-1}$  (Figure S5E), which is 10 times lower than the previously used scan rate. At this scan rate the shape of the CV curve in the TEMPO groups oxidation region becomes close to a cathodic wave with a limiting current plateau, typical for low scan rate CV of a reversible redox pair in solution. The mass growth for one deposition cycle is ca.  $0.3\text{ }\mu\text{g cm}^{-2}$  both for  $5\text{ mVs}^{-1}$  and  $50\text{ mVs}^{-1}$  CVs. Polymer deposition is observed both at potentials higher than  $0.8\text{ V}$  and lower than  $0.4\text{ V}$ , and during low rate CV almost two thirds of the overall polymer mass is formed at potentials more positive than the potentials of the A/A' peaks. On the contrary, at  $50\text{ mV/s}$  only one third of the polymer is formed at potentials higher than  $0.8\text{ V}$ . This indicates that the Coulombic shielding from oxidized TEMPO groups allows coupling between the radical cations of DiTS and the charged TEMPO groups, though at quite low rate. The possibility of polymerization at both potential regions was confirmed by the experiment consisting of a series of successive iterations of potentiostatic and potentiodynamic syntheses, as well as open-circuit rest periods (See SI and Figure S6 for further discussion).

An XPS spectrum, obtained for the polymeric film, confirmed the presence of the functional groups, typical for the backbone and the pendant groups (Figure S9).

Continuous-wave EPR (cwEPR) measurements were performed to examine the nitroxyl fragments of DiTS before and

after electrochemical polymerization. X-band ( $\sim 9.4\text{ GHz}$ ) cwEPR spectra were recorded for a powder sample containing the DiTS monomer as well as for a polymerized DiTS film at room temperature. The spectra are shown in Figure 3. The g-factor was found to be between 2.006 and 2.007 as expected for the nitroxyl fragments, consistent with literature values for TEMPOL radicals.<sup>[23]</sup> In contrast to the spectrum of dilute TEMPOL in solution, which exhibits three lines due to the hyperfine interaction between the electron spin of the radical and the N nucleus with spin 1 (not shown), we observe only a single broad resonance line for both samples. This single broadened line results from the strong exchange interaction between neighboring nitroxyl groups caused by the high concentration of spins in the DiTS powder as well as in the polymerized film. The linewidth of the DiTS monomer signal is smaller than the linewidth observed for the p-DiTS film, suggesting a smaller exchange interaction between the TEMPO fragments in the film.

In order to assess the amount of active nitroxyl groups in the film, an average number of spins per monomer unit was determined using quantitative EPR (qEPR) measurements as described previously.<sup>[24]</sup> The average number of active spins in the DiTS powder sample was found to be 2.20 spins per molecule. For the polymerized DiTS film monomer deposited on a gold electrode on a quartz substrate, the number of spins was found to be 1.75 spins per monomer unit. This indicates that, within the measurement error of approximately 20%, the nitroxyl fragments remain intact during the electrochemical polymerization.

### 2.3. Electrochemical Performance

The electrochemical properties of p-DiTS were studied by cyclic voltammetry (Figure 4A) and galvanostatic charge-discharge techniques (Figure 4B). The electrochemical behavior of p-DiTS films was found to be insensitive to the change of the electrode material, so further experiments were carried out on glassy carbon electrodes. The peaks associated with the NiSalen backbone and the TEMPO pendants overlap, which confirms

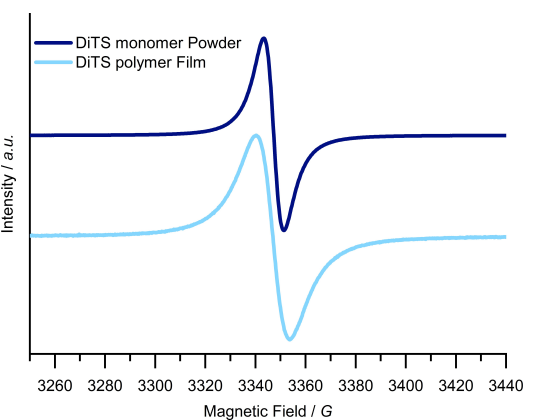


**Figure 3.** Room-temperature cwEPR spectra of a DiTS monomer sample and an electropolymerized p-DiTS film.

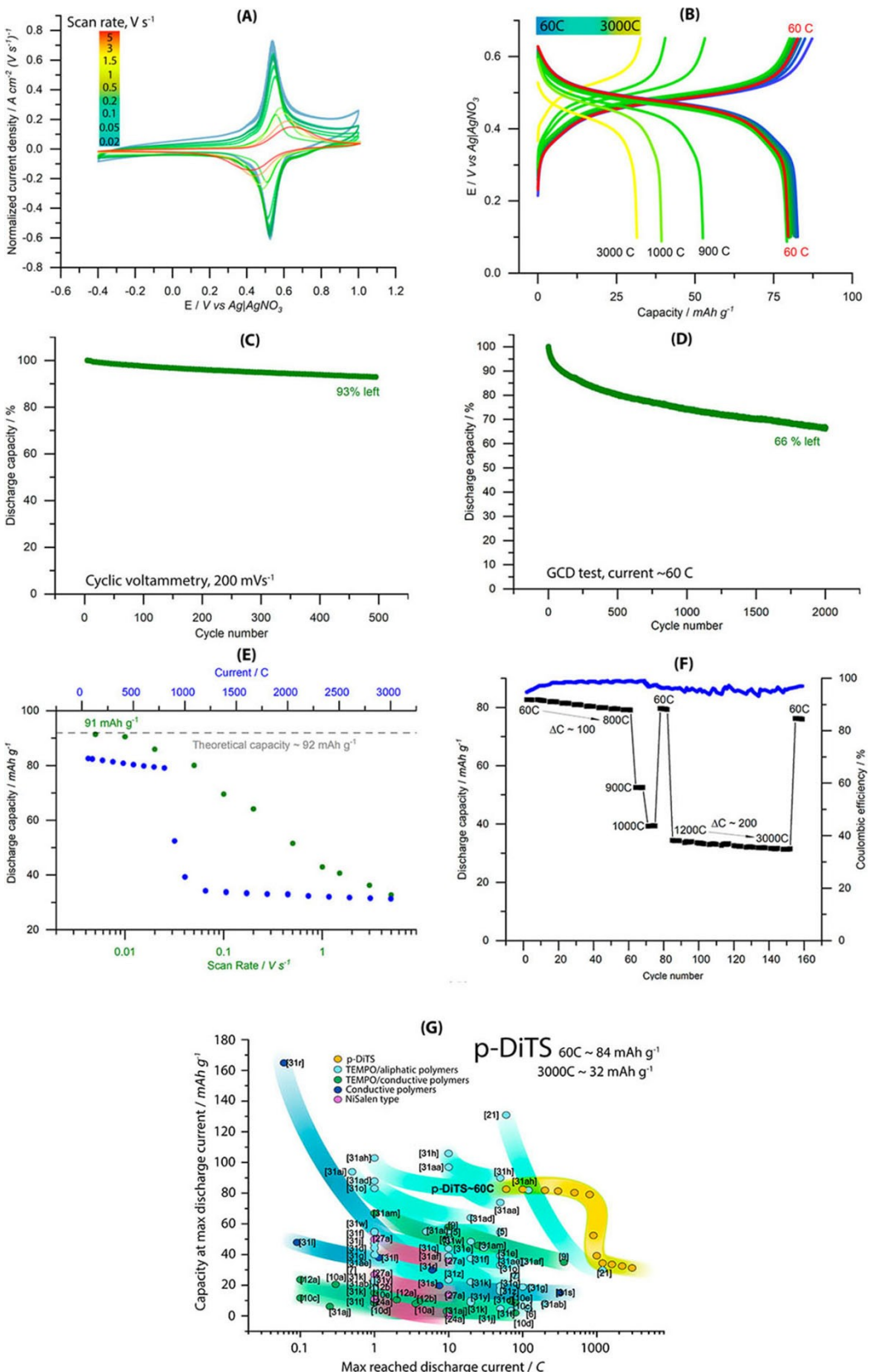


**Figure 4.** CV of thin film of the polymer p-DiTS (A) and specific capacity (E) measured in 0.1 M Et<sub>4</sub>NBF<sub>4</sub> / CH<sub>3</sub>CN solution using various potential sweep rates; The CV stability of p-DiTS during long-term measurements in 0.1 M Et<sub>4</sub>NBF<sub>4</sub>/CH<sub>3</sub>CN solution with 200 mV s<sup>-1</sup> scan rate (C). Charge/discharge test of p-DiTS using different currents (B, F) and stability test at I ~ 60 C (D) in 0.1M Et<sub>4</sub>NBF<sub>4</sub>/CH<sub>3</sub>CN solution; Comparison of energy storage properties of most common TEMPO-containing materials and conducting polymers (G).<sup>[4–9,10,12a–c,21,27a,29,31]</sup>

perfect redox matching of the fragments, but impedes the separation of the individual signals (Figure 4A). However, the main peaks are attributed to redox transformations of the TEMPO groups, while the shoulders, usually not observed for aliphatic TEMPO-containing polymers, correspond to processes involving the NiSalen backbone. The onset of NiSalen backbone oxidation is located at 0.2 V, and the electroactivity of this fragment is observed till 0.8 V. Wide and flat CV, typical for substituted NiSalen, such as poly[Ni(CH<sub>3</sub>O)Salen]<sup>[27]</sup>, should correspond to 1 electron transitions, while TEMPO groups give 2 electrons in DiTS. We can roughly divide the DiTS voltammogram by pseudocapacitive-type CV, connected by the straight lines the shoulders, attributed to the NiSalen backbone redox reaction (area 1-1'), and redox polymer CV with peaks 2, 2', corresponding to TEMPO fragments redox processes (Figure S7). The area under the CV parts is proportional to the charge consumed in each redox process. The estimated areas for the NiSalen and TEMPO parts match a ratio of 1:1.65, which is close to the theoretical ratio of 1:2, expected from the molecular structure.

A proportionality between the peak currents and the potential scan rate is observed for scan rates up to 200 mV s<sup>-1</sup> (Figure S8, A), where the current-rate dependence changes from linear to square root behavior, as seen from the log-log plots of both the anodic and the cathodic peak current vs scan rate. This indicates a transition from a diffusion-less "thin layer model" electrochemical behavior of the film to a semi-infinite diffusion control at higher scan rates.<sup>[25]</sup> The apparent rate constants and the standard electrode potential of the redox processes in p-DiTS were calculated from the dependence of the peak potential on the logarithm of the potential sweep rate using a standard method (Figure S8B).<sup>[26]</sup> The resulting apparent rate constant, ~6.5 s<sup>-1</sup>, is indicative of extremely fast kinetics,<sup>[26b]</sup> which might be partially due to the open structure of p-DiTS supporting fast mass transport through the material and close distance between TEMPO groups, facilitating electron exchange.

Specific capacities of p-DiTS were determined using CV in wide scan-rate range (green line, Figure 4E). At a scan rate of 5 mV s<sup>-1</sup> this material gains 91.5 mAh g<sup>-1</sup>, closely approaching the theoretical capacity of 92 mAh g<sup>-1</sup> for three electrons transferred per monomeric unit (one electron from the NiSalen backbone and one from each pendant group). This result puts p-DiTS into a good position among other known TEMPO modified polymers (Figure 4G) and significantly exceeds the capacity of unmodified NiSalen complexes.<sup>[27]</sup> The capacity remained unchanged up to 20 mV s<sup>-1</sup> and then gradually decreased to 32.7 mAh g<sup>-1</sup> with increasing scan rate up to 5000 mV s<sup>-1</sup>. The CV cycling stability curve of p-DiTS at 200 mV s<sup>-1</sup> (Figure 4C) demonstrates the retention of 93% of the initial capacity after 500 cycles. Our results demonstrate the remarkable stability of p-DiTS in comparison to NiSalen type polymers (20% loss after 500 cycles).<sup>[28]</sup>

The performance of p-DiTS as a cathode material was studied in a half-cell by means of GCD (Figure 4B) using a symmetrical current for charging and discharging for C-rates between 60 C and 3000 C (78 μA cm<sup>-2</sup> to 3.94 mA cm<sup>-2</sup> respec-

tively, assuming 1 C current to be 100 mA g<sup>-1</sup>). The discharge curves for p-DiTS exhibit a slightly inclined plateau at ca. 0.53 V, indicative of TEMPO-based redox processes, and sloped regions at 0.30–0.40 V corresponding to NiSalen based redox processes (Figure 4B). It should be noted that the charge curve has the same median voltage as the discharge curve, thus leading to a close to unity charge-discharge energy efficiency. The specific capacity of the p-DiTS films reached 83 mAh g<sup>-1</sup> at a current equal to 60 C and was roughly constant until 800 C (79 mAh g<sup>-1</sup>, Figure 4F and E), dropping sharply to 39 mAh g<sup>-1</sup> at 1000 C and to 31 mAh g<sup>-1</sup> at 3000 C. The capacity drop was found to be reversible and restores (79–80 mAh g<sup>-1</sup>) upon further cycling at 60 C. Long-term cyclability of p-DiTS was also tested by the GCD method at a rate of 60 C in 0.1 M Et<sub>4</sub>NBF<sub>4</sub> / CH<sub>3</sub>CN solution (Figure 4D). The material demonstrates notable durability retaining 66% of its specific capacity after 2000 cycles of GCD with the Coulombic efficiency of the process about 95%, thus demonstrating superior stability as compared to NiSalen type polymers<sup>[27a]</sup> and TEMPO-containing materials at GCD tests.<sup>[10c,29]</sup> To the best of our knowledge, such a combination of extra-fast charge-discharge, high capacity and good durability is encountered for the first time among other TEMPO-containing polymers (Figure 4G and Table S1). An electrochemical cell with p-DiTS as active cathode material was constructed for in-situ EPR experiments. Using this cell, we were able to study the EPR signals associated with paramagnetic states in p-DiTS as a function of the applied electrical potential. Figure 5A shows EPR spectra of the oxidized and reduced p-DiTS film in a 0.1 M Et<sub>4</sub>NBF<sub>4</sub>/CH<sub>3</sub>CN solution. The significant decrease in the TEMPO signal intensity observed upon oxidizing the p-DiTS film indicates that a substantial fraction of the TEMPO groups can be actively oxidized. A precise description of the in-situ EPR setup as well as a quantitative analysis of the spin concentration in the p-DiTS film as a function of the applied potential will be the subject of a future publication.

Further insight into the charge/discharge mechanism in p-DiTS was provided by advanced electrochemical and spectroscopic techniques. An EQCM study of ion transport associated with charging/discharging of the p-DiTS film allowed us to establish the anionic nature of the ion transport in p-DiTS (Figure 5B and C). A mass flux of charge compensating ions was determined from the slope in the linear regions of the mass/charge dependence (Figure 5C).<sup>[30]</sup> BF<sub>4</sub><sup>-</sup> could be identified as the main charge compensating ions. Their intercalation compensates the positive charge in the p-DiTS film, confirming the p-type nature of p-DiTS.<sup>[32]</sup>

Operando electronic conductance of p-DiTS films was studied using interdigitated electrodes with a bipotentiostat in CV mode. The dependence of the p-DiTS conductance on the applied potential was found to be typical for NiSalens<sup>[20]</sup> and other conductive polymers,<sup>[33]</sup> showing a narrow conductivity window with a peak conductivity of 1.75 mSm at 0.55 V. This value is more than 3 orders of magnitude higher than the value beyond the conductivity window (ca. 10 μSm) (Figure 5D). Such a high conductivity value surpasses the conductance of aliphatic TEMPO-based polymers, such as PTMA, by almost two

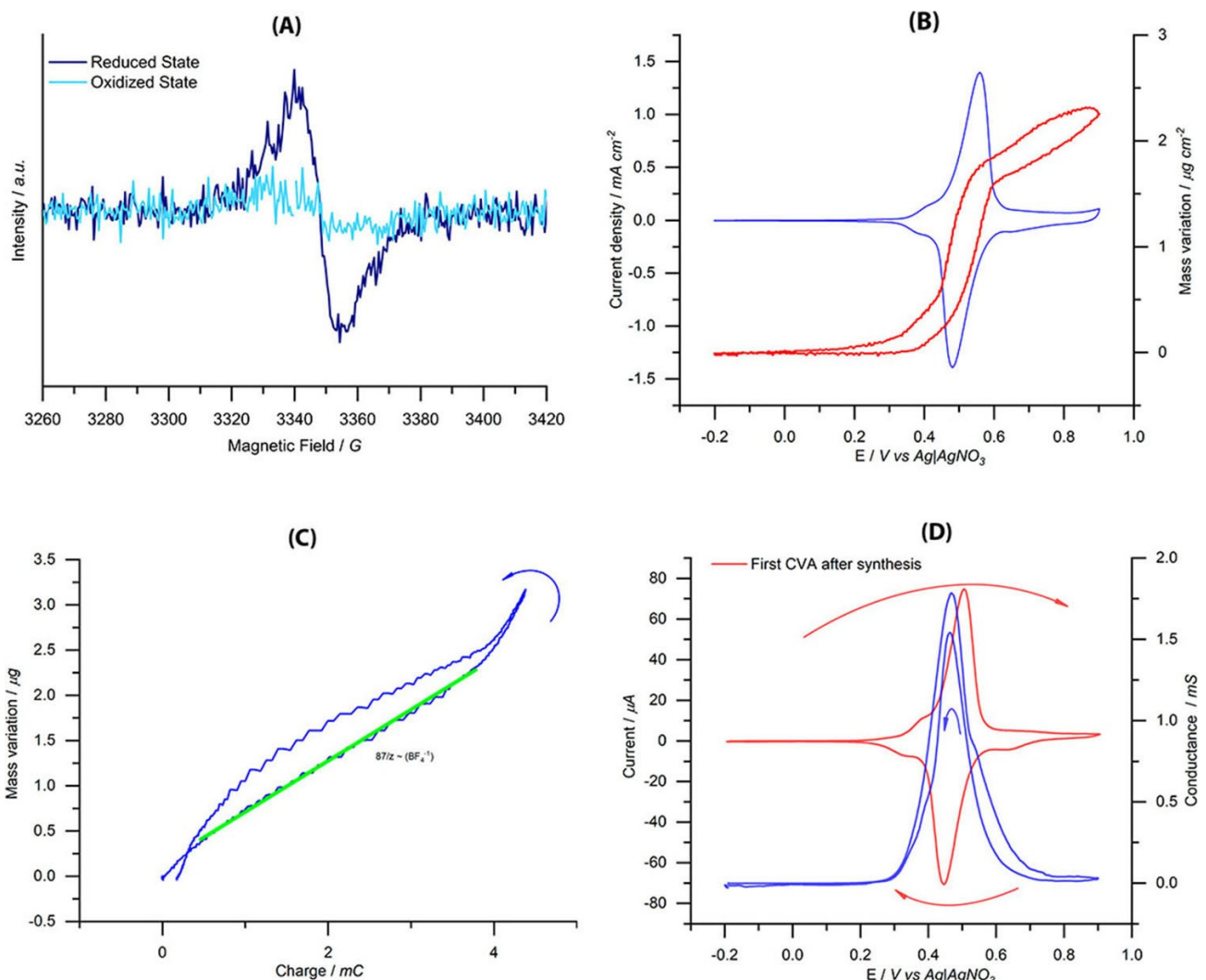


**Figure 5.** Operando EPR spectra of p-DiTS for the oxidized and reduced states (A). EQCM of a quartz crystal coated by p-DiTS with changes of the polymer film mass (B), dependencies of the polymer film mass on the oxidation charge (C). The scan direction is indicated by the arrows. The measurement was performed in 0.1 M Et<sub>4</sub>NBF<sub>4</sub>/CH<sub>3</sub>CN solution. The conductivity of p-DiTS measured using interdigitated electrode arrays in an electrolyte (D) recorded during CV with 5 mV s<sup>-1</sup>. The electrolyte was 0.1 M Et<sub>4</sub>NBF<sub>4</sub>/CH<sub>3</sub>CN.

orders of magnitude. The conductance of p-DiTS thus approaches the conductance of NiSalen polymers measured under identical conditions.<sup>[20,34]</sup>

SEM images of as-prepared p-DiTS films show loose and porous morphology similar to NiSalen materials,<sup>[19g,22]</sup> which provides high permeability of porous films to the electrolyte and ensures sufficient ionic conductivity. After oxidation, most of the cavities were filled (Figure 6B), indicating an intercalation of charge-compensating ions.

The p-DiTS oxidation mechanism was revealed using operando spectroelectrochemical studies. UV-Vis spectra of the film were recorded during stepwise oxidation in the range between -0.20 and 1.00 V. Several potential-dependent absorption bands (Figure 7B and C) were found, corresponding to different species in the macromolecule. In the reduced state of the polymer (until 0.3 V, Figure 7A), when the doping level is low, the absolute spectra exhibit several absorption bands (Figure 7B) that are typical for polymeric NiSalen complexes.<sup>[35]</sup>

Upon further oxidation, significant spectral changes were noticed, as seen from the different UV-Vis spectra (Figure 7C) and normalized absorbance curves (Figure 7D).

Absorption at  $\lambda_{\max} \approx 316$  nm, assigned to the intervalence charge transfer (IVCT) of the 4,4'-dihydroxybiphenyl dianion (Figure 7E) naturally decreased in intensity during the whole course of the oxidation (Figure 7D). The bands at  $\lambda_{\max} \approx 350$ –402 nm (Figure 7D) are assigned to the  $\pi$ - $\pi^*$  electronic transition in the phenoxy ring (the transition between the valence and antibonding polaron level or between the bonding and antibonding polaron levels).<sup>[36]</sup> The bands at  $\lambda_{\max} \approx 805$  nm, assigned to the transition from the valence band to the bonding polaron level at the Ni(salen) backbone oxidation,<sup>[37]</sup> increased with the moderate potential (from 0.3 to 0.8 V), but decreased with further oxidation (Figure 7D). All bands increase in intensity during step-by-step oxidation, except for the 316 nm band, because of the rising population of polarons (Figure 7D). This fact reveals that the electron conductive

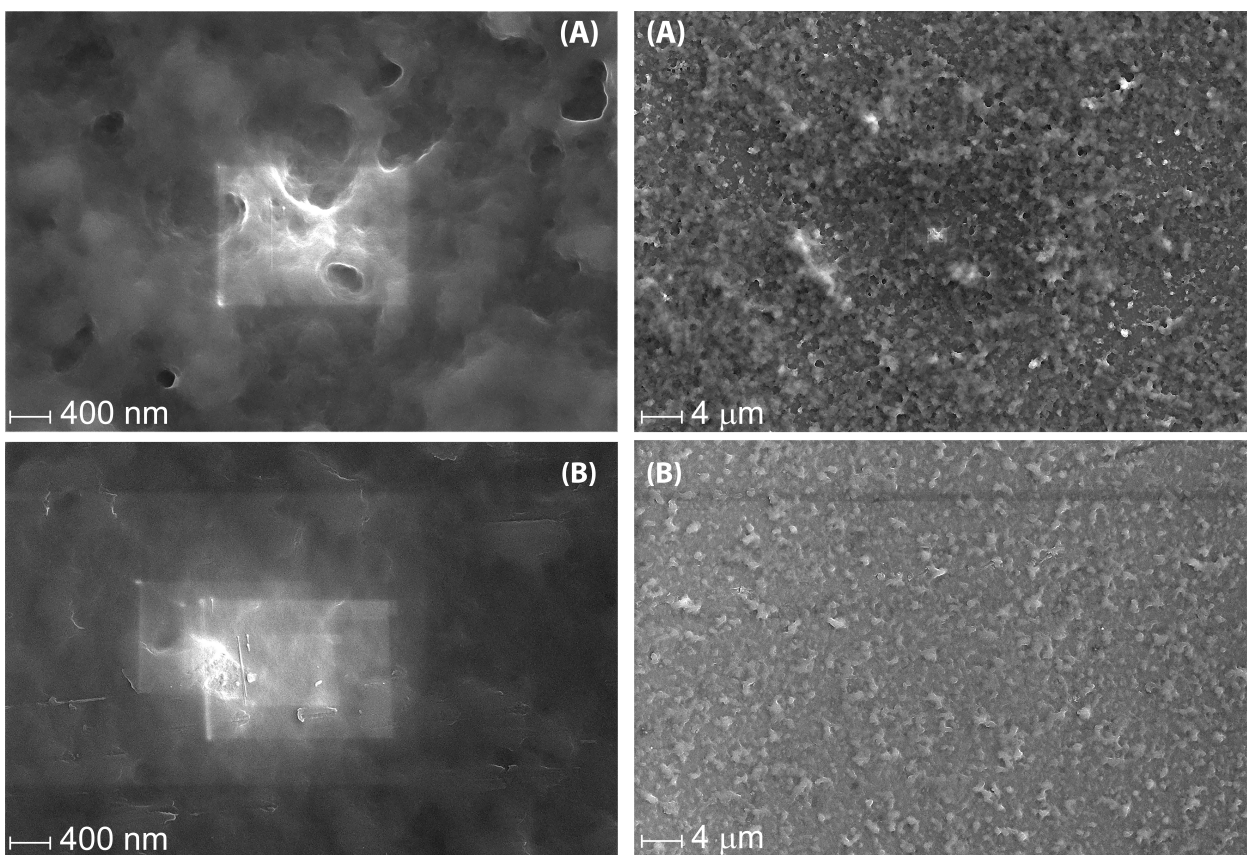


Figure 6. SEM images for thin films of p-DiTS in reduced (A) and oxidized (B) states.

backbone of p-DiTS takes part in the oxidation process. Keeping in mind that the maximum conductivity was observed in the range between 0.4 and 0.55 V, corresponding to the region of maximum absorption, one may conclude that the polaronic pathway makes the major contribution to the material conductivity. At the end of the oxidation process, i.e. near the highest level of doping (Figure 7E), a new absorption band appears at ca.  $\lambda_{\text{max}} \approx 495$  nm (Figure 7C and D). At high anodic potential (higher than 0.9 V), a new highly delocalized bi-polaron  $\pi$  system may appear through the quinoid bond between two phenyl rings, leading to a decrease in other polaron bands, and is related to a charge transfer transition between the Ni and the new  $\pi$  electronic structure of the NiSalen type ligand.<sup>[36]</sup> The absolute spectra show the presence of a band ( $\lambda_{\text{max}} \approx 470$  nm) apparently associated with TEMPO radical and cation states in reduced and oxidized states of the polymer respectively.<sup>[38]</sup> The intensity of these bands also increases during oxidation (small area of green line between 0.4 and 0.65 V, Figure 7D) due to the rising population of  $\text{TEMPO}^+$  cations. However, the extinction coefficient for the TEMPO group is much lower than the coefficient for NiSalen type molecules ( $10.5\text{--}20.3 \text{ M}^{-1} \text{ cm}^{-1}$  vs  $90\text{--}170 \text{ M}^{-1} \text{ cm}^{-1}$  respectively)<sup>[32,38]</sup> which leads to the low intensity of the TEMPO band in the spectra (Figure 7B)

### 3. Conclusions

In conclusion, we have presented the successful design and synthesis of p-DiTS, the first example of a NiSalen-based nitroxyl CRP material. Electrochemical anodic deposition of this polymer from  $\text{CH}_3\text{CN}$  solution of the corresponding monomer was shown to proceed in an unusual manner, with the polymerization occurring mostly after partial reduction of the previously oxidized film. CV experiments show perfect redox matching between the nitroxyl groups and the NiSalen backbone such that nearly all TEMPO fragments contribute to the charging/discharging process. This is confirmed by operando UV-Vis and EPR studies.

The observed electrochemical behavior results in an unexpectedly high performance of p-DiTS: the maximum specific capacity is as high as  $91.5 \text{ mAh g}^{-1}$  for a discharge rate of  $5 \text{ mV s}^{-1}$ , which is close to the theoretical capacity ( $92 \text{ mAh g}^{-1}$ ). Unlike most nitroxyl-based materials, p-DiTS retains its significant capacity at extremely high discharge rates ( $82 \text{ mAh g}^{-1}$  at  $60^\circ\text{C}$ ,  $79 \text{ mAh g}^{-1}$  at  $800^\circ\text{C}$ ,  $39 \text{ mAh g}^{-1}$  at  $1000^\circ\text{C}$  and  $31 \text{ mAh g}^{-1}$  at  $3000^\circ\text{C}$ ) and shows a good cycling stability (66% capacity retention after 2000 cycles). Overall, the proposed strategy for the adjustment of the redox matching between the nitroxyl radicals and the NiSalen conductive backbone allows for exploiting the full potential of the material and ensures extraordinarily high electron-transport rates,

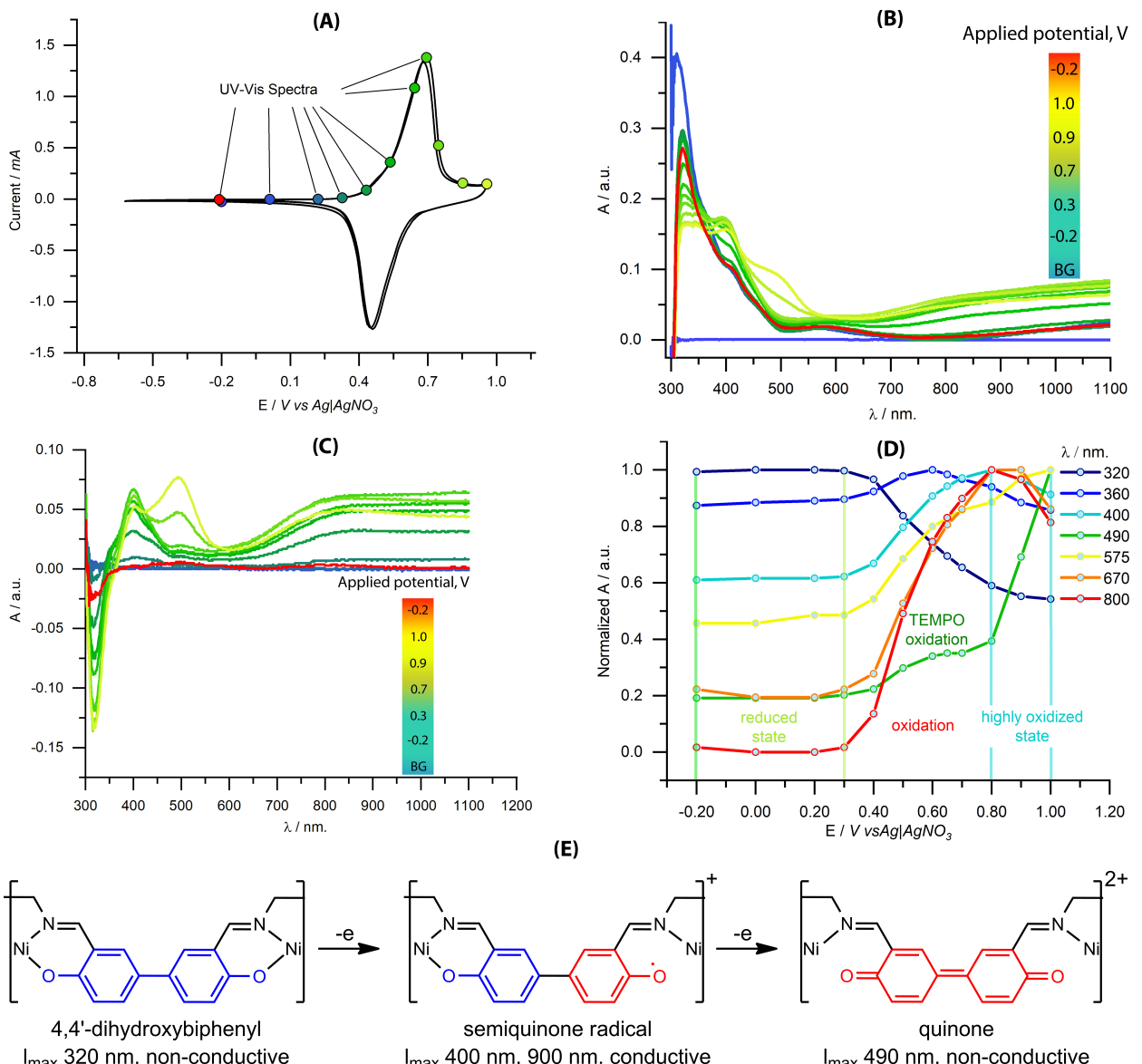


**Figure 7.** Electronic spectra of p-DiTS deposited on ITO a glass substrate covered with ITO. Absolute spectra recorded *in situ* for potentials in the range of -0.2 – 1.0 V (B), CV of p-DiTS for the same potentials as in (A), spectra with a reference to the neutral polymer (C) and normalized dependence of the absorbance on the potential (D). A scheme of matching the UV signals and polymer states (E). The background electrolyte is a 0.1 M Et<sub>4</sub>NBF<sub>4</sub>/CH<sub>3</sub>CN solution.

providing a powerful tool for the construction of organic electrode materials for next-generation hybrid supercapacitors and organic batteries.

## Acknowledgements

Scientific research was partially performed at the Center for Geo-Environmental Research and Modelling (GEOMODEL), Chemistry Educational Center, Interdisciplinary Center for Nano-technology, Center for Chemical Analysis and Materials Research, Research Center for Magnetic Resonance of Research park of St. Petersburg State University. All EPR measurements were carried out at the Berlin Joint EPR Lab, Freie Universität Berlin. The synthetic work and energy storage properties of the material were made with

support by the Russian Science Foundation, grant # 16-13-00038. Analysis of the charge transfer mechanism was performed with support by RFBR, project number # 20-33-90122. Conductivity tests with relevant analysis were supported by the Russian Science Foundation, grant # 19-19-00175. EPR measurements were supported by the German-Russian Interdisciplinary Science Center (G-RISC) funded by the German Federal Foreign Office via the German Academic Exchange Service (DAAD). Academic exchange between Saint-Petersburg State University and Freie Universität Berlin was supported by a Joint Seed Funding Project of SPbU and FUB, grant # 39855834.

## Conflict of Interest

The authors declare no conflict of interest.

**Keywords:** polymers · conducting materials · electrochemistry · ultra-fast recharge materials · organic radical battery

- [1] S. Muench, A. Wild, C. Friebe, B. Haupler, T. Janoschka, U. S. Schubert, *Chem. Rev.* **2016**, *116*, 9438–9484.
- [2] T. Janoschka, M. D. Hager, U. S. Schubert, *Adv. Mater.* **2012**, *24*, 6397–6409.
- [3] K. Nakahara, S. Iwasa, M. Satoh, Y. Morioka, J. Iriyama, M. Suguro, E. Hasegawa, *Chem. Phys. Lett.* **2002**, *359*, 351–354.
- [4] K. Koshiba, N. Sano, K. Oyaizu, H. Nishide, *Chem. Commun. (Camb.)* **2009**, 836–838.
- [5] J.-K. Kim, *J. Power Sources* **2013**, *242*, 683–686.
- [6] A. Vlad, J. Rolland, G. Hauffman, B. Ernould, J. F. Gohy, *ChemSusChem* **2015**, *8*, 1692–1696.
- [7] C.-H. Lin, J.-T. Lee, D.-R. Yang, H.-W. Chen, S.-T. Wu, *RSC Adv.* **2015**, *5*, 33044–33048.
- [8] J. Xiang, R. Burges, B. Häupler, A. Wild, U. S. Schubert, C.-L. Ho, W.-Y. Wong, *Polymer* **2015**, *68*, 328–334.
- [9] K. Oyaizu, H. Tatsuhira, H. Nishide, *Polym. J.* **2014**, *47*, 212–219.
- [10] a) S. Bahceci, B. Esat, *J. Power Sources* **2013**, *242*, 33–40; b) T. Katsumata, M. Satoh, J. Wada, M. Shiotsuki, F. Sanda, T. Masuda, *Macromol. Rapid Commun.* **2006**, *27*, 1206–1211; c) J. Qu, T. Katsumata, M. Satoh, J. Wada, T. Masuda, *Macromolecules* **2007**, *40*, 3136–3144; d) J. Qu, T. Fujii, T. Katsumata, Y. Suzuki, M. Shiotsuki, F. Sanda, M. Satoh, J. Wada, T. Masuda, *J. Polym. Sci. Part A* **2007**, *45*, 5431–5445; e) J. Qu, T. Katsumata, M. Satoh, J. Wada, J. Igarashi, K. Mizoguchi, T. Masuda, *Chemistry* **2007**, *13*, 7965–7973.
- [11] a) L. Xu, F. Yang, C. Su, L. Ji, C. Zhang, *Electrochim. Acta* **2014**, *130*, 148–155; b) L. Xu, P. Guo, H. He, N. Zhou, J. Ma, G. Wang, C. Zhang, C. Su, *Ionics* **2017**, *23*, 1375–1382; c) F. Li, S. Wang, Y. Zhang, J. L. Lutkenhaus, *Chem. Mater.* **2018**, *30*, 5169–5174.
- [12] a) M. Aydin, B. Esat, Ç. Kılıç, M. E. Köse, A. Ata, F. Yilmaz, *Eur. Polym. J.* **2011**, *47*, 2283–2294; b) M. Aydin, B. Esat, *J. Solid State Electrochem.* **2015**, *19*, 2275–2281; c) P.-O. Schwartz, M. Pejic, M. Wachtler, P. Bäuerle, *Synth. Met.* **2018**, *243*, 51–57; d) F. Li, D. N. Gore, S. Wang, J. L. Lutkenhaus, *Angew. Chem. Int. Ed. Engl.* **2017**, *56*, 9856–9859.
- [13] C. Karlsson, H. Huang, M. Strømme, A. Gogoll, M. Sjödin, *RSC Adv.* **2015**, *5*, 11309–11316.
- [14] R. B. Araujo, A. Banerjee, P. Panigrahi, L. Yang, M. Strømme, M. Sjödin, C. M. Araujo, R. Ahuja, *J. Mater. Chem. A* **2017**, *5*, 4430–4454.
- [15] I. A. Chepurnaya, P. V. Gaman'kov, T. Y. Rodyagina, S. V. Vasil'eva, A. M. Timonov, *Russ. J. Electrochem.* **2003**, *39*, 314–317.
- [16] F. Deng, X. Li, F. Ding, B. Niu, J. Li, *J. Phys. Chem. C* **2018**, *122*, 5325–5333.
- [17] O. V. Levin, M. P. Karushev, A. M. Timonov, E. V. Alekseeva, S. Zhang, V. V. Malev, *Electrochim. Acta* **2013**, *109*, 153–161.
- [18] C. Freire, M. Nunes, C. Pereira, D. M. Fernandes, A. F. Peixoto, M. Rocha, *Coord. Chem. Rev.* **2019**, *394*, 104–134.
- [19] a) J. Li, F. Gao, Y. Zhang, F. Kang, X. Wang, F. Ye, J. Yang, *Science China Chemistry* **2012**, *55*, 1338–1344; b) Y. Zhang, J. Li, F. Gao, F. Kang, X. Wang, F. Ye, J. Yang, *Electrochim. Acta* **2012**, *76*, 1–7; c) J.-I. Li, F. Gao, Y.-k. Zhang, X.-d. Wang, *Chin. J. Polym. Sci.* **2010**, *28*, 667–671; d) F. Gao, J. Li, Y. Zhang, X. Wang, F. Kang, *Electrochim. Acta* **2010**, *55*, 6101–6108; e) F. Gao, J. Li, F. Kang, Y. Zhang, X. Wang, F. Ye, J. Yang, *J. Phys. Chem. C* **2011**, *115*, 11822–11829; f) X. Li, F. Deng, J. Li, Z. Li, F. Kang, *Electrochim. Acta* **2018**, *284*, 355–365; g) E. V. Alekseeva, I. A. Chepurnaya, V. V. Malev, A. M. Timonov, O. V. Levin, *Electrochim. Acta* **2017**, *225*, 378–391.
- [20] A. A. Vereshchagin, P. S. Vlasov, A. S. Konev, P. Yang, G. A. Grechishnikova, O. V. Levin, *Electrochim. Acta* **2019**, *295*, 1075–1084.
- [21] K. Koshiba, N. Sano, K. Oyaizu, H. Nishide, *Macromol. Chem. Phys.* **2009**, *210*, 1989–1995.
- [22] M. V. Novozhilova, E. A. Smirnova, M. P. Karushev, A. M. Timonov, V. V. Malev, O. V. Levin, *Russ. J. Electrochem.* **2016**, *52*, 1183–1190.
- [23] A. Clark, J. Sedhom, H. Elajaili, G. R. Eaton, S. S. Eaton, *Concepts Magn. Reson. Part A* **2016**, *45* A.
- [24] P. Pingel, M. Arvind, L. Kölln, R. Steyrleuthner, F. Krafft, J. Behrends, S. Janietz, D. Neher, *Adv. Electron. Mater.* **2016**, *2*.
- [25] M. Vilas-Boas, C. Freire, B. d. Castro, A. R. Hillman, *J. Phys. Chem. B* **1998**, *102*, 8533–8540.
- [26] a) E. Laviron, *J. Electroanal. Chem. Interfacial Electrochem.* **1979**, *101*, 19–28; b) M. Sterby, R. Emanuelsson, X. Huang, A. Gogoll, M. Strømme, M. Sjödin, *Electrochim. Acta* **2017**, *235*, 356–364.
- [27] a) S. N. Eliseeva, E. V. Alekseeva, A. A. Vereshchagin, A. I. Volkov, P. S. Vlasov, A. S. Konev, O. V. Levin, *Macromol. Chem. Phys.* **2017**, *218*; b) J.-I. Li, F. Gao, Y.-k. Zhang, X.-d. Wang, *Chin. J. Polym. Sci.* **2010**, *28*, 667–671; c) C. Chen, X. Li, F. Deng, J. Li, *RSC Adv.* **2016**, *6*, 79894–79899.
- [28] E. V. Alekseeva, V. A. Ershov, A. S. Konev, O. V. Levin, *ECS Trans.* **2018**, *87*, 167–177.
- [29] a) T. Katsumata, J. Qu, M. Shiotsuki, M. Satoh, J. Wada, J. Igarashi, K. Mizoguchi, T. Masuda, *Macromolecules* **2008**, *41*, 1175–1183; b) T. Suga, H. Ohshiro, S. Sugita, K. Oyaizu, H. Nishide, *Adv. Mater.* **2009**, *21*, 1627–1630.
- [30] S. A. Krasikova, M. A. Besedina, M. P. Karushev, E. A. Dmitrieva, A. M. Timonov, *Russ. J. Electrochem.* **2010**, *46*, 218–226.
- [31] a) L.-f. Deng, X.-h. Li, L.-x. Xiao, Y.-h. Zhang, *J. Cent. South Univ. Technol.* **2003**, *10*, 190–194; b) T. Suga, K. Yoshimura, H. Nishide, *Macromol. Symp.* **2006**, *245*–*246*, 416–422; c) L. Bugnon, C. J. H. Morton, P. Novak, J. Vetter, P. Nesvadba, *Chem. Mater.* **2007**, *19*, 2910–2914; d) J. Kim, G. Cheruvally, J. Choi, J. Ahn, S. Lee, D. Choi, C. Song, *Solid State Ionics* **2007**, *178*, 1546–1551; e) J.-K. Kim, G. Cheruvally, J.-W. Choi, J.-H. Ahn, D. S. Choi, C. E. Song, *J. Electrochem. Soc.* **2007**, *154*; f) K. Nakahara, J. Iriyama, S. Iwasa, M. Suguro, M. Satoh, E. J. Cairns, *J. Power Sources* **2007**, *163*, 1110–1113; h) T. Suga, H. Konishi, H. Nishide, *Chem. Commun. (Camb.)* **2007**, *1730*–*1732*; i) M. Suguro, S. Iwasa, Y. Kusachi, Y. Morioka, K. Nakahara, *Macromol. Rapid Commun.* **2007**, *28*, 1929–1933; j) J.-K. Kim, G. Cheruvally, J.-H. Ahn, Y.-G. Seo, D. S. Choi, S.-H. Lee, C. E. Song, *Journal of Industrial and Engineering Chemistry* **2008**, *14*, 371–376; k) S. H. Lee, J.-K. Kim, G. Cheruvally, J.-W. Choi, J.-H. Ahn, G. S. Chauhan, C. E. Song, *J. Power Sources* **2008**, *184*, 503–507; l) H.-S. Min, B. Y. Park, L. Taherabadi, C. Wang, Y. Yeh, R. Zaouk, M. J. Madou, B. Dunn, *J. Power Sources* **2008**, *178*, 795–800; m) J. Qu, F. Z. Khan, M. Satoh, J. Wada, H. Hayashi, K. Mizoguchi, T. Masuda, *Polymer* **2008**, *49*, 1490–1496; n) J. Qu, R. Morita, M. Satoh, J. Wada, F. Terakura, K. Mizoguchi, N. Ogata, T. Masuda, *Chemistry* **2008**, *14*, 3250–3259; o) M. Suguro, S. Iwasa, K. Nakahara, *Macromol. Rapid Commun.* **2008**, *29*, 1635–1639; p) X. Zhang, H. Li, L. Li, G. Lu, S. Zhang, L. Gu, Y. Xia, X. Huang, *Polymer* **2008**, *49*, 3393–3398; q) J.-K. Kim, J.-H. Ahn, G. Cheruvally, G. S. Chauhan, J.-W. Choi, D.-S. Kim, H.-J. Ahn, S. H. Lee, C. E. Song, *Met. Mater. Int.* **2009**, *15*, 77–82; r) Z. Mandić, M. K. Roković, T. Pokupčić, *Electrochim. Acta* **2009**, *54*, 2941–2950; s) G. Nyström, A. Razaq, M. Strømme, L. Nyholm, A. Mihranyan, *Nano Lett.* **2009**, *9*, 3635–3639; t) J. Qu, T. Katsumata, M. Satoh, J. Wada, T. Masuda, *Polymer* **2009**, *50*, 391–396; u) M. Suguro, A. Mori, S. Iwasa, K. Nakahara, K. Nakano, *Macromol. Chem. Phys.* **2009**, *210*, 1402–1407; v) J.-Z. Wang, S.-L. Chou, H. Liu, G. X. Wang, C. Zhong, S. Yen Chew, H. Kun Liu, *Mater. Lett.* **2009**, *63*, 2352–2354; w) T. Ibe, R. B. Frings, A. Lachowicz, S. Kyo, H. Nishide, *Chem. Commun. (Camb.)* **2010**, *46*, 3475–3477; x) K. Koshiba, N. Chikushii, N. Sano, K. Oyaizu, H. Nishide, *Green Chem.* **2010**, *12*; y) Y. Dai, Y. Zhang, L. Gao, G. Xu, J. Xie, *J. Electrochem. Soc.* **2011**, *158*; z) H.-C. Lin, C.-C. Li, J.-T. Lee, *J. Power Sources* **2011**, *196*, 8098–8103; aa) Y. H. Wang, M. K. Hung, C. H. Lin, H. C. Lin, J. T. Lee, *Chem. Commun. (Camb.)* **2011**, *47*, 1249–1251; ab) W. Guo, Y.-X. Yin, S. Xin, Y.-G. Guo, L.-J. Wan, *Energy Environ. Sci.* **2012**, *5*, 5221–5225; ac) M.-K. Hung, Y.-H. Wang, C.-H. Lin, H.-C. Lin, J.-T. Lee, *J. Mater. Chem.* **2012**, *22*, 1570–1577; ad) Y. Kim, C. Jo, J. Lee, C. W. Lee, S. Yoon, *J. Mater. Chem.* **2012**, *22*, 1453–1458; ae) C. M. Liu, J. Chen, F. Q. Wang, B. L. Yi, *Russ. J. Electrochem.* **2012**, *48*, 1052–1057; af) I. S. Chae, M. Koyano, T. Sukegawa, K. Oyaizu, H. Nishide, *J. Mater. Chem. A* **2013**, *1*; ag) G. Hauffman, Q. Maguin, J. P. Bourgeois, A. Vlad, J. F. Gohy, *Macromol. Rapid Commun.* **2014**, *35*, 228–233; ah) T. Sukegawa, I. Masuko, K. Oyaizu, H. Nishide, *Macromolecules* **2014**, *47*, 8611–8617; ai) B. Ernould, M. Devos, J.-P. Bourgeois, J. Rolland, A. Vlad, J.-F. Gohy, *J. Mater. Chem. A* **2015**, *3*, 8832–8839; aj) S. B. Sertkol, D. Sinirligil, B. Esat, A. E. Miftuooglu, *J. Polym. Res.* **2015**, *22*; ak) T. Sukegawa, K. Sato, K. Oyaizu, H. Nishide, *RSC Adv.* **2015**, *5*, 15448–15452; al) K. Takahashi, K. Korolev, K. Tsuji, K. Oyaizu, H. Nishide, E. Bryuzgin, A. Navrotskiy, I. Novakov, *Polymer* **2015**, *68*, 310–314; am) J. Xiong, Z. Wei, T. Xu, Y. Zhang, C. Xiong, L. Dong, *Polymer* **2017**, *130*, 135–142.

- [32] V. V. Sizov, M. V. Novozhilova, E. V. Alekseeva, M. P. Karushev, A. M. Timonov, S. N. Eliseeva, A. A. Vanin, V. V. Malev, O. V. Levin, *J. Solid State Electrochem.* **2014**, *19*, 453–468.
- [33] J. Heinze, B. A. Frontana-Uribe, S. Ludwigs, *Chem. Rev.* **2010**, *110*, 4724–4771.
- [34] E. V. Beletskii, Y. A. Volosatova, S. N. Eliseeva, O. V. Levin, *Russ. J. Electrochem.* **2019**, *55*, 339–345.
- [35] E. Dmitrieva, M. Rosenkranz, J. S. Danilova, E. A. Smirnova, M. P. Karushev, I. A. Chepurnaya, A. M. Timonov, *Electrochim. Acta* **2018**, *283*, 1742–1752.
- [36] J. Tedim, S. Patrício, J. Fonseca, A. L. Magalhaes, C. Moura, A. R. Hillman, C. Freire, *Synth. Met.* **2011**, *161*, 680–691.
- [37] K. Łępicka, P. Pieta, A. Shkurenko, P. Borowicz, M. Majewska, M. Rosenkranz, S. Avdoshenko, A. A. Popov, W. Kutner, *J. Phys. Chem. C* **2017**, *121*, 16710–16720.
- [38] J. B. Gerken, S. S. Stahl, *ACS Cent. Sci.* **2015**, *1*, 234–243.

---

Manuscript received: September 16, 2020  
Revised manuscript received: October 28, 2020  
Accepted manuscript online: November 17, 2020  
Version of record online: November 27, 2020

---